ME525 Applied Acoustics Lecture 12, Winter 2024
Combining monopoles and dipoles:
The Helmholtz-Kirchhoff (H-K) integral
An exact solution to the H-K integral

Peter H. Dahl, University of Washington

Superposition of point sources

Using the free space Green's function representing a source at $\vec{r}_0$

$$g = \frac{1}{4\pi}\frac{e^{ik|\vec{r}-\vec{r}_0|}}{|\vec{r}-\vec{r}_0|} \tag{1}$$

we can find the total pressure for a superposition of n point sources (Fig. 1) as

$$p(r) = \frac{q_1}{4\pi}\frac{e^{ik|\vec{r}-\vec{r}_1|}}{|\vec{r}-\vec{r}_1|} + \frac{q_2}{4\pi}\frac{e^{ik|\vec{r}-\vec{r}_2|}}{|\vec{r}-\vec{r}_2|} + ... + \frac{q_n}{4\pi}\frac{e^{ik|\vec{r}-\vec{r}_n|}}{|\vec{r}-\vec{r}_n|} \tag{2}$$

allow the source strength for the n source to be q_n, with $e^{-i\omega t}$ time dependence assumed. (Note also that a different frequency ω can be used for each of the n sources.)

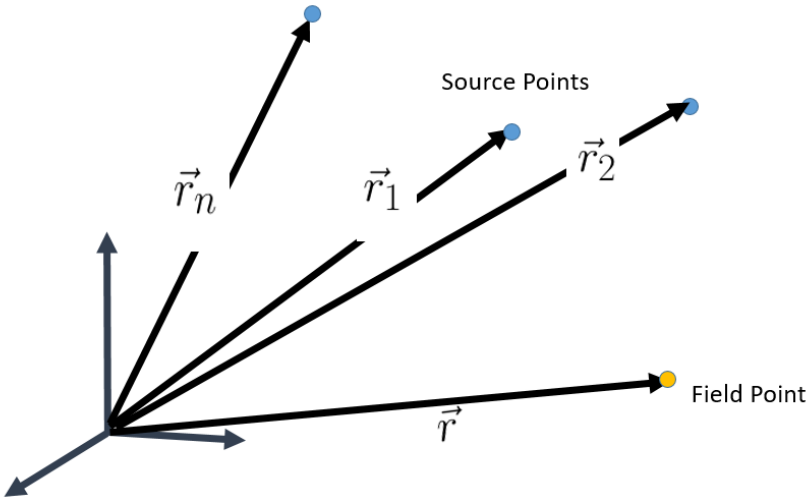

Figure 1: Superposition of n point sources composing the total acoustic pressure at the field point $\vec{r}$

Similarly, there can be continuous distribution of point sources found within a volume V_s–like a sphere filled with marbles each being a point source–with any particular source at $\vec{r}_s$ having a source strength $q(\vec{r}_s)$. In this case the total pressure is the integral over the volume V_s

$$p(r) = \int_{V_s} q(\vec{r}_s)g(\vec{r},\vec{r}_s)dV_s \tag{3}$$

recalling the notation that $g(\vec{r},\vec{r}_s)$ is Eq.(1) with $\vec{r}_0 = \vec{r}_s$. Do a quick check: if the source distribution consisted of one discrete source, say at position $\vec{r}_0$ inside the volume, then $q(\vec{r}_s) = q\delta(\vec{r}_s - \vec{r}_0)$, and integral over V_s yields $p(r) = qg(\vec{r},\vec{r}_0)$ in view of the sifting property of the delta function.

A vibratory surface consisting of a surface distribution of elementary sources

Next apply the superposition principle to construct a surface distribution of sources. Figure 2 depicts a vibrating 3D surface of spherical shape generating sound. As a first attempt, model sound generation by a surface distribution of monopole sources with constant velocity amplitude on the surface such that the elemental pressure due to a single patch of surface dS located at $\vec{r}_s$ is

$$dp = -i\omega\rho_0 u_n(\vec{r}_s)g(\vec{r},\vec{r}_s)dS \tag{4}$$

where $u_n(\vec{r}_s)$ is the normal velocity on the surface at $\vec{r}_s$. Notice that for this problem we have suspended use of source strength q in favor of an explicit value of the normal acceleration $-i\omega u_n(\vec{r}_s)$ times surface area dS. However, do look back onto the discussion in Lecture 8, where the concept of q was introduced and confirm that q has the same dimension as $-i\omega u_n(\vec{r}_s)dS$, i.e., the elemental dS takes on the role of sphere area a^2.

The thick, black line (arrow) in Fig. 2 represents the vector $\vec{r}-\vec{r}_s$ connecting one of the monopole sources related to surface area dS located at $\vec{r}_s$ (or source point) to some arbitrary field point $\vec{r}$. (These $\vec{r}_s$ and $\vec{r}$ vectors are not explicity shown but would be associated with a coordinate system as in Fig. 1.)

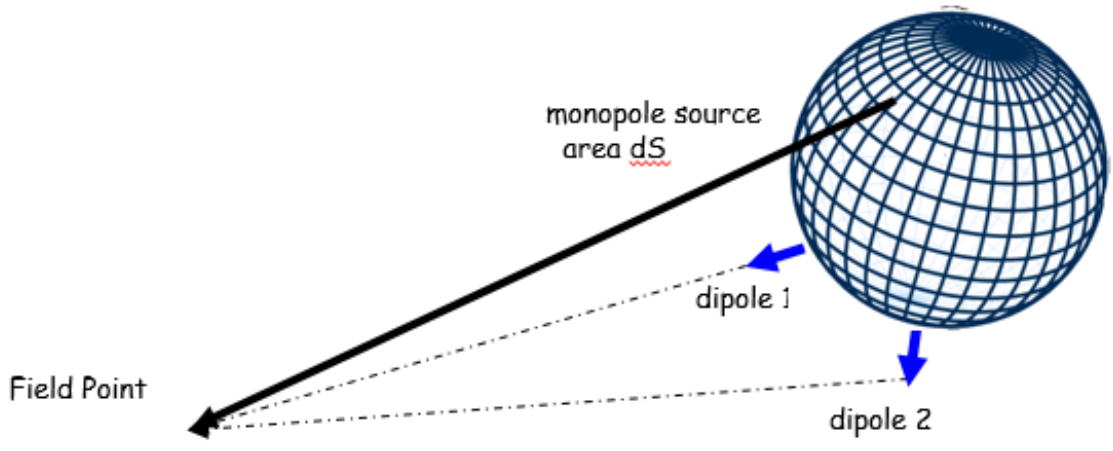

Figure 2: Spherical sound source consisting of surface distribution of elementary sources. Radiation from one monopole elementary source to a field point is shown by solid black line; radiation from two dipole elementary sources is shown by the dotted lines.

It would be really convenient if we could just find the total pressure radiated from this source by integrating over the surface S, or basically summing up all the elemental pressure contributions dp from each dS as follows:

$$p_m(\vec{r}) = \int_S -i\omega\rho_0 u_n(\vec{r}_s) g(\vec{r}, \vec{r}_s) dS \tag{5}$$

where the subscript m ties this pressure to a distribution of monopoles over surface S. This is indeed possible for some geometries which leads to an approach of very practical use, however, for an arbitrary 3D vibrating surface as in Fig. 2, Eq.(5) does not give the complete story.

But for such a non-planer surface of high curvature there will in general will be a need for surface distribution of dipole sources. The two thin, dashed lines sepresent the vectors $\vec{r} - \vec{r}_s$ connecting two different dipole sources. Both dipoles have their axes normal to the surface, but dipole 1 is expected to contribute more to the total pressure at the field point owing to the orientation of the dipole axis with the field point. The problem lies in the fact that when distributed over such a highly curved surface as in Fig. 2, elemental vibrating sources as in monopoles each with contribution dp, cannot assume to be in isolation and operating in free space. This is because other parts of surface S tend to shadow, reflect, and otherwise exert an influence by generating a pressure distribution on the surface of the vibrating body $p(\vec{r}_s)$ that must be accounted for (Fahy 2001, Tempkin 2001).

Such an accounting is made by including a distribution of elemental dipole sources as follows:

$$p_d(\vec{r}) = \int_S p(\vec{r}_s) \frac{\partial g}{\partial n} dS \tag{6}$$

where the subscript d ties this pressure to a distribution of dipoles over surface S.

Now take the integral in Eq.(5) about monopole surface source, plus the integral in Eq.(6) about dipole surface sources, and combine them. The results is new integral, Eq.(7) for finding the pressure at a field point $\vec{r}$ based on this surface distribution of dipoles (first term) and monopoles (second term). Thus the total pressure can be written as follows:

$$p(\vec{r}) = \int_S [p(\vec{r}_s) \frac{\partial g}{\partial n} - i\omega\rho_0 u_n(\vec{r}_s) g(\vec{r}, \vec{r}_s)] dS \tag{7}$$

This is known as the *Helmholtz-Kirchhoff integral*.

The Helmholtz-Kirchhoff (H-K) integral poses many challenges to solving. One reason is the first integral is generally more difficult to evaluate than the second. Also, in many instances one may not know the strength of each dipole which is defined by, or linked to, the surface pressure $p(\vec{r}_s)$ at that same position.

For example, a vibrating surface, such as an engine (Fig. 3) might be modeled with constant harmonic velocity amplitude on the engine surface, u_o, associated with engine vibration (i.e, an

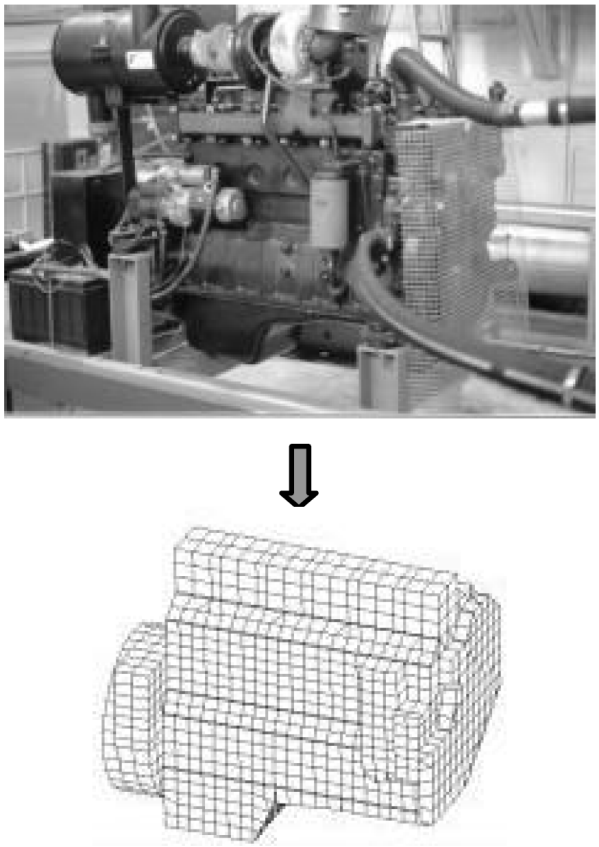

Figure 3: Boundary mesh for the boundary integral method (BEM) analysis for study of noise emission from a diesel engine. This is Fig. 5 from D. W. Herrin *et al.*

acceleration amplitude of ωu_o.) Modeling sound radiation from the engine thus involves the H-K integral with $u_n(\vec{r}_s)$ on the engine surface set to u_o. However this does not necessarily specify the surface pressure $p(\vec{r}_s)$ and the H-K integral needs to be recast as an integral equation for $p(\vec{r}_s)$ and generally solved numerically. Often this is a very difficult challenge; some numerical approaches include the boundary element method or BEM.

In ME525 we instead move forward with a more simple, but extremely practical, alternative to summing elemental sources over an area of a radiating surface, known as the *Rayleigh Integral*.

But let's not leave the H-K integral quite yet as is instructive to both drill down a bit more on the differential pressure associated with the dipole contribution, and also study an example exact solution. This will help to better inform us on the appropriate usage of the Rayleigh integral.

Within the H-K integral the dipole moment vector as part of an elemental source at some position on the surface $\vec{r}_s$ cannot take just any orientation but must align with the outward normal $\vec{n}$ at position $\vec{r}_s$ on the surface. A quick explanation for this is that the dipole strength must come from the pressure at that specific point, $p(\vec{r}_s)$, which can only act normally on the surface, hence the dipole moment vector must also be normal to the surface.

For the surface in Fig. 2, the two dipoles are shown at different locations and dipole moment

vectors (blue arrows) are shown aligned with the surface normal at these locations. To obtain the pressure at the field point the dot product of the moment vectors with the corresponding $\vec{r} - \vec{r}_s$ vectors (dotted lines in Fig. 2) is needed, and on this basis it is easy to see that dipole 2 contributes much less than dipole 1 owing to the much smaller dot product.

The differential pressure associated with the dipole contribution is,

$$dp = p(\vec{r}_s)\frac{\partial g}{\partial n}dS. \tag{8}$$

Confirm yourself that Eq.(8) has correct dimension, given that $\frac{\partial g}{\partial n}$ is the spatial derivative of g with respect to an outward normal $\vec{n}$ at position $\vec{r}_s$ on the surface. For the surface dipoles in Fig. 2, identify $[p(\vec{r}_s)dS]\vec{n}$ with the dipole moment vector $\vec{f}_D$ first discussed in context of an isolated dipole (Lecture 11). Note further that $\vec{n} \cdot \nabla g = \frac{\partial g}{\partial n}$. It may also be useful in some cases to use

$$\frac{\partial g}{\partial n} = \cos\alpha \frac{\partial g}{\partial R}dS \tag{9}$$

where $R = |\vec{r} - \vec{r}_s|$, with $\frac{\partial g}{\partial R} = \frac{e^{ikR}}{4\pi R}(ik - \frac{1}{R})$. Using this we can again see the interpretation of the angle α between the dipole moment vector and the vector connecting dipole source location with the field point (Fig. 3, Lecture 11).

In summary, think of sound radiation from a general 3D body, as in the sphere shown in Fig. 2 in terms of the H-K integral as a superposition of monopole and dipole sources distributed over the entire, radiating area, of the 3D body. The monopole contribution will have strength $-i\omega\rho_0 u_n(\vec{r}_s)dS$ depending on the particular location $\vec{r}_s$, and each source contribution is propagated to the field point via g which is function of field point $\vec{r}$ and $\vec{r}_s$. The dipole contribution will have strength $p(\vec{r}_s)dS$, propagated to the field point via $\frac{\partial g}{\partial n}$, also a function of $\vec{r}$ and $\vec{r}_s$. By inspection of the basic geometry, e.g., as the case in Fig. 2, one can intuit that many dipole contributions will have little or no effect depending on the orientation of the dipole source with the particular $\vec{r} - \vec{r}_s$ vector.

An exact solution to the Helmholtz-Kirchhoff integral: radiation from a sphere

We next provide an exact solution to the Helmholtz-Kirchhoff integral for a problem we have solved earlier via a much simpler means: radiation from a sphere of radius a vibrating with constant amplitude over its surface. The problem solved (Lecture 4) involved the specification of a constant velocity on the spherical surface at $r = a$, equal to $u_0 e^{-i\omega t}$, where u_0 is a complex amplitude, hence the vibration or acceleration amplitude is $-i\omega u_0$, and we've seen this problem multiple times in homework. The solution is

$$p(r,t) = a\rho_0 c\ \frac{u_0}{r}e^{ik(r-a)}(\frac{ka}{ka+i})e^{-i\omega t} \tag{10}$$

Why do this again? Hopefully the exercise should convince you that the Helmholtz-Kirchhoff integral really works, and one can truly describe sound radiation from a vibrating body as an appropriate sum of monopoles and dipoles. Furthermore, exact, canonical, problems like this can be used as "benchmark" solutions to compare results of more complicated numerical codes.

The H-K integral is Eq.(11) where S is the surface of a sphere of radius a, and the constant u_0 replaces a generally variable normal velocity $u_n(\vec{r}_s)$ on the surface at $\vec{r}_s$

$$p(\vec{r}) = \int_S [p(\vec{r}_s)\frac{\partial g}{\partial n} - i\omega\rho_0 u_0 g(\vec{r},\vec{r}_s)]dS. \tag{11}$$

There is an unknown pressure over the surface of the sphere $p(\vec{r}_s)$, but symmetry demands that $p(\vec{r}_s)$ not take on any value different from any other value (e.g., as it can for the diesel engine shown in Lecture 11), so it is set to the constant $p(a)$. However this constant pressure value remains unknown and it will have to be determined eventually.

To take further advantage of symmetry, a coordinate system is placed at the center of the sphere (Fig. 4) Now break up the H-K integral, and deal with second integral first, call it I_m

$$I_m = \int_S g(\vec{r},\vec{r}_s)dS \tag{12}$$

which upon multiplication by $-i\omega\rho_0 u_0$ gives the acoustic field from a uniform distribution of monopole sources over the surface of the sphere.

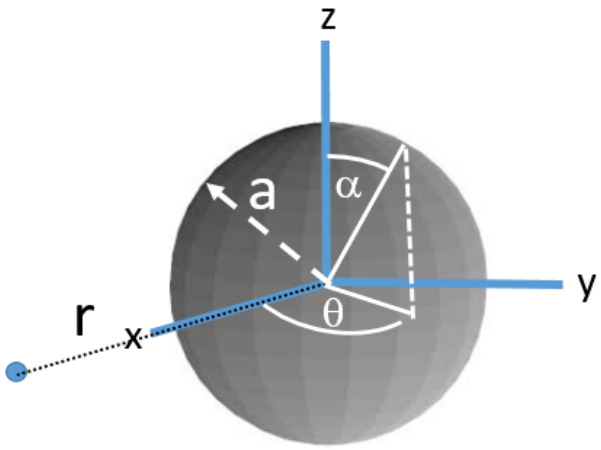

Figure 4: A spherical source of radius a placed at the center of the Cartesian coordinate system (x,y,z). Because of spherical symmetry, one spherical coordinate r describes all variation.

Since the field at point $\vec{r}$ doesn't show angular variation owing to symmetry, a good strategy then is to identify a field point at range r located to be located on one of the Cartesian axes. Set this

point to be on the x-axis with $\vec{r} = \begin{bmatrix} r \\ 0 \\ 0 \end{bmatrix}$, and owing to symmetry this point represents *any* field point.

Now introduce polar angle α and azimuthal angle θ, then all source points $\vec{r}_s$ are described using $\vec{r}_s = \begin{bmatrix} a\sin\alpha\cos\theta \\ a\sin\alpha\sin\theta \\ a\cos\alpha \end{bmatrix}$. Next put $R = |\vec{r} - \vec{r}_s| = \sqrt{r^2 + a^2 - 2ar\cos\alpha}$, and I_m can be reduced to

$$I_m = 2\pi a^2 \int_0^\pi \sin\alpha \frac{e^{ikR}}{R} d\alpha \tag{13}$$

This is readily evaluated, e.g., put $W = \cos\alpha$, $dW = -\sin\alpha d\alpha$, giving

$$I_m = a\sin(ka)\frac{e^{ikr}}{kr}. \tag{14}$$

Unfortunately, $-i\omega\rho_0 u_0 I_m$ is not the complete solution. Interestingly, try evaluating both $-i\omega\rho_0 u_0 I_m$ and the known exact solution of Eq.(10) in the $ka << 1$ limit, and find that they are equivalent. Why is that?

Now return to the first integral in Eq. (11), call this I_d because it is the dipole contribution. The unknown pressure on the surface of sphere $p(a)$ can be taken outside the integral, given that we at least know it is a constant, and expressing $\frac{\partial g}{\partial n}$ as $\nabla g \cdot \vec{n}$ then

$$I_d = \int_S \nabla g \cdot \vec{n} dS \tag{15}$$

where $p(a)I_d$ gives the acoustic field from a uniform distribution of dipole sources over the surface of the sphere.

The divergence theorem is used to convert the surface integral over the surface of the sphere into a volume integral over the volume V of the sphere, of $\nabla^2 g$. But now recall that

$$\nabla^2 g + k^2 g = -\delta(|\vec{r} - \vec{r_s}|) \tag{16}$$

Now equate $\nabla^2 g$ to $-k^2 g - \delta(|\vec{r} - \vec{r_s}|)$ and instead integrate these terms over the volume V.

But there are no receiver points, or field points, *inside* the sphere, since we are solving the problem for field points $\vec{r}$ *outside* of the sphere, or $r > a$. Thus, the argument $|\vec{r} - \vec{r_s}|$ *never* becomes 0 inside the volume V and by the definition of the delta function, the volume integral of $\delta(|\vec{r} - \vec{r_s}|)$ will be 0. Thus $I_d = -k^2 \int_V g dV$. Apart from the k^2 factor, I_d describes a volume V (of the sphere) now filled with point monopole sources, at source points $\vec{r}_s$ within the sphere, as result of applying

the divergence theorem.

To proceed put $R = |\vec{r} - \vec{r}_s| = \sqrt{r^2 + \rho^2 - 2\rho r \cos\alpha}$, where ρ varies from 0 to a, and I_d becomes

$$I_d = \frac{1}{2}\int_0^a \rho^2 d\rho \int_0^\pi \sin\alpha \frac{e^{ikR}}{R} d\alpha. \tag{17}$$

The integral over α can is more easily solved by putting $w = \cos\alpha$, $d\alpha = \frac{-dw}{\sin\alpha}$ after which you should arrive (maybe try it yourself?) at

$$I_d = (ka\cos ka - \sin ka)\frac{e^{ikr}}{kr} \tag{18}$$

Now, observe that evaluating Eq.(11) at a field point on the surface of the $\vec{r} = a$ (but not inside the sphere), implies

$$p(a) = p(a)I_d(a) - i\omega\rho_0 u_0 I_m(a) \tag{19}$$

and find the unknown pressure $p(a)$ equal to

$$p(a) = \frac{-i\omega\rho_0 u_0 I_m(a)}{1 - I_d(a)} \tag{20}$$

with complete solution

$$p(r) = p(a)I_d(r) - i\omega\rho_0 u_0 I_m(r) \tag{21}$$

the first term being the dipole contribution and the second being the monopole contribution.

Everything in Eq. (21) is represented by the simple formula given in Eq.(10), for the problem we already solved. With more algebraic manipulation they equate precisely. Instead its more interesting to keep it as it is, broken out into its dipole and monopole terms; plot them out and see if the coherent sum matches Eq. (10).

This is done (Fig. 5) for a sphere of radius $a = 0.05$ m, for which there is a uniform velocity amplitude on the surface of the sphere of $u_0 = 0.001$ m/s. The velocity has harmonic dependence $e^{-i\omega t}$. Results are computed for a frequency that stepped through from 10 Hz to 20000 Hz in 10 Hz steps. This establishes a range of ka (using c = 330 m/s), which goes from values $<< 1$ to about 20. The mean-square pressure is plotted at range 1 m for the monopole term (red line), dipole term (blue line), their sum (black, dashed line), and the exact solution (green line) using of Eq. (10).

It should be clear that Eq.(21) works, and we have successfully modeled acoustic emission from a spherical source in terms of a surface distribution of dipoles of strength $p(a)$, and a surface distribution of monopoles of strength $-i\omega\rho_0 u_0$. It's interesting to see that at some particular values of ka either just the monopole or dipole term approximates the exact solution in Eq.(10) reasonably well, as in $ka \sim 9.3$ for the monopole and $ka \sim 11$ for the dipole, with this behavior being periodic ka. Additionally for ka less than about 0.2 the complete solution is well satisfied by the just the

monopole term.

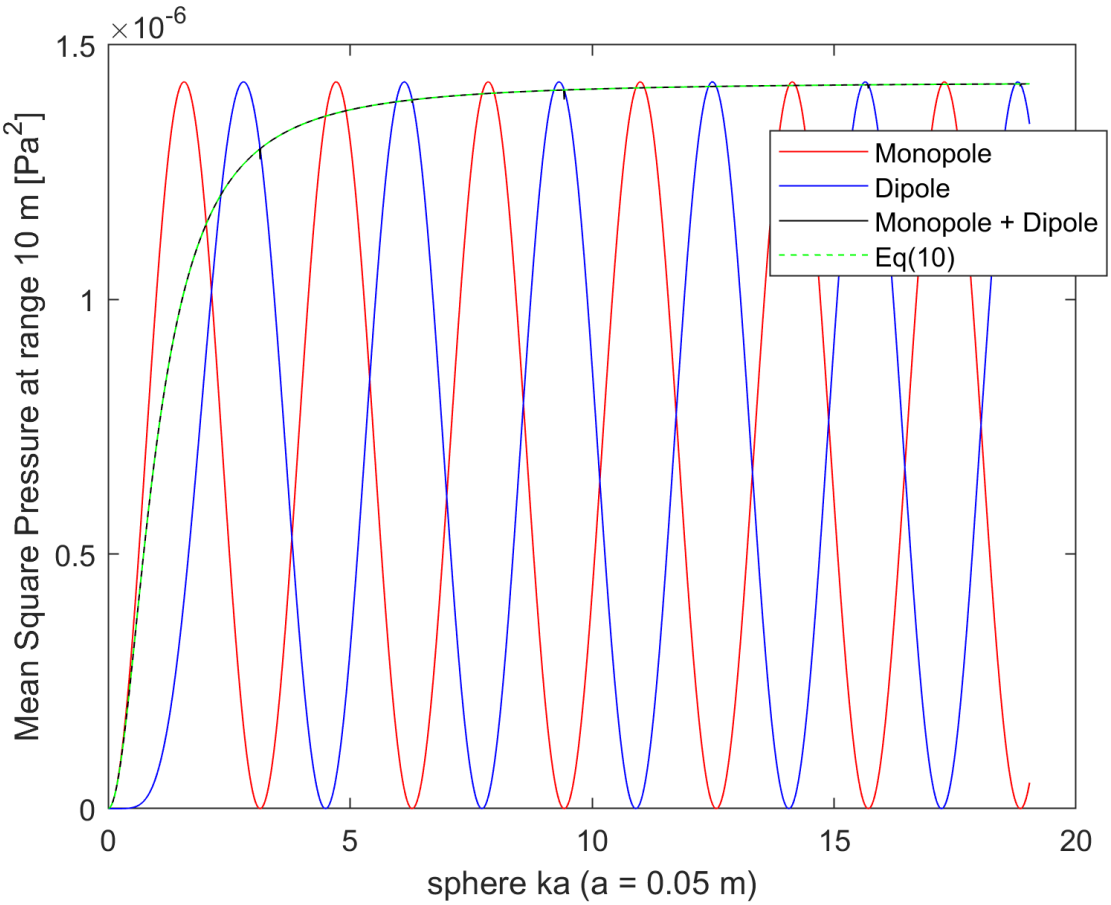

Figure 5: Mean square pressure at range 10 m associated with sound radiation from a sphere of radius $a = 0.05$ m, vibrating with uniform velocity amplitude on the surface of the sphere $u_0 = 0.001$ m/s. Results are plotted as function of ka which is varied by increasing the frequency from 10 Hz to 20000 Hz. The pressure is expressed in terms of a monopole contribution (red line), dipole contribution (blue line) and exact solution (dashed green line) via Eq. (10). Combining the monopole and dipole distributions through Eq.(21) also gives the exact solution.

We are done with the H-K integral in terms of ME525 involvement. More complicated geometries with curvature but without the kind symmetry we see in this problem, must be solved numerically such as the boundary element method (BEM).

However, if the surface is relatively flat one can imagine that each dipole on the surface, with dipole axis aligned with the local surface normal, will pretty much cancel itself out. Thus the I_d part of the H-K integral can be neglected, in favor of doing the computationally simpler I_m integral. This is the basis behind the Rayleigh integral discussed next and which you will have an opportunity to work with.

References

F. Fahy, *Foundations of Engineering Acoustics* (Elsevier Academic Press, San Diego, CA, 2001)

Temkin, S. *Elements of Acoustics*,(Acoustical Society of America, and American Institute of Physics, 2001)
D. W. Herrin *et al.* "New Look at the High Frequency Boundary Element and Rayleigh Integral Approximation" Soc. of Automotive Eng. O3NVC-114, 2003

ME525 Applied Acoustics Lecture 13 Winter 2024
The Rayleigh integral, beam patterns, hydrodynamic and geometric near and far fields

Peter H. Dahl, University of Washington

Rayleigh integral

We have now studied the Helmholtz-Kirchhoff integral , Eq.(1), to compute the sound radiation from a surface S based on a generally variable normal velocity $u_n(\vec{r}_s)$ over the surface at position $\vec{r}_s$ plus a similarly varying pressure distribution $p(\vec{r}_s)$ which can depend in complicated way on $u_n(\vec{r}_s)$. (Where once again $p(\vec{r},t) = p(\vec{r})e^{-i\omega t}$.)

$$p(\vec{r}) = \int_S [p(\vec{r}_s)\frac{\partial g}{\partial n} - i\omega\rho_0 u_n(\vec{r}_s)g(\vec{r},\vec{r}_s)]dS \tag{1}$$

Solution of Eq.(1) poses difficult numerical challenges, primarily involving finding the unknown pressure distribution $p(\vec{r}_s)$. In some problems, such as sound radiation from a spherical source of fixed radius a, the relation between $p(\vec{r}_s)$ and $u_n(\vec{r}_s)$ is worked out and the integral solved exactly.

If there are situations where the first integral in Eq.(1) can be ignored, the solution is greatly simplified. Fortunately, this happens in many situations where the radiation surface S is planar (or at least approximately so), as was first demonstrated by Rayleigh (see Junger and Feit, 1993).

To understand how this happens we introduce the concept of a *baffle* where there is a limited portion of the planar surface that is vibrating and generating sound, while the remaining portion of the surface idealized as rigid. The baffle within which the aperture (or sound radiating part) is set (Fig. 1) theoretically extends to infinity in all directions and restricts the sound field to only one hemisphere but otherwise does not vibrate.

The boundary condition on the aperture is such that it is impenetrable to sound, and reflects sound completely. This means pressure on such a boundary will double (as if someone talking very close to a hard wall- try it yourself), rather than pressure going to zero as observed from sound below an air-water interface. The result of this reasoning is such that the first term of the Helmoltz-Kirchhoff equation is eliminated and the second term is increased by a factor of two (Pierce, 1989)

Now write formally the Rayleigh integral as

$$p(\vec{r}) = -i2\omega\rho_0 \int_S u_n(\vec{r}_s)g(\vec{r},\vec{r}_s)dS. \tag{2}$$

For the planar geometries involved in evaluating the Rayleigh integral, a Cartesian coordinate sys-

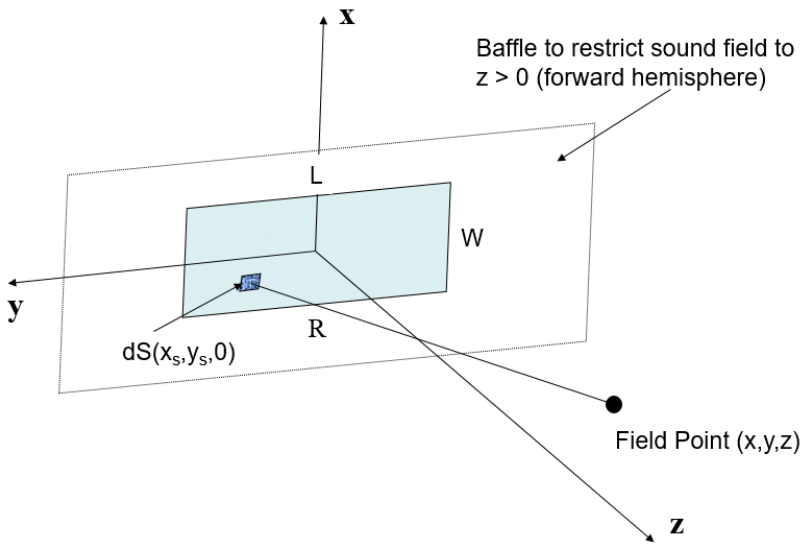

Figure 1: Cartesian coordinate system established at the center of radiating rectangular aperture confined by a baffle to restrict the sound field to $z > 0$. The elemental source dS is distance R from the field point where $R = \sqrt{(x - x_s)^2 + (y - y_s)^2 + z^2}$

tem centered on the radiating aperture (Fig. 1) is best, where

$$p(\vec{r}) = \frac{-i\omega\rho_0}{2\pi} \int_S u_n(x_s, y_s) \frac{e^{ikR}}{R} dx_s dy_s \tag{3}$$

with $R = |\vec{r} - \vec{r}_s|$.

Next we relax the definition of a baffle that extends to infinity, and even relax (somewhat) the criterion that the aperture be perfectly flat. Figure 2 shows two planar-like radiating apertures and associated baffles that are used on small, autonomous underwater vehicles (AUV). Notice these are slightly curved to match the hull curvature of the AUV. Furthermore. knowing the characteristic length scales of aperture, as in L and W in Fig. 2, combined with sound frequency to give kW and kL will yield much information without having to lift a finger!

We often encounter situations that simplify the computation even further, such as in Fig. 3 where $W < L$ and $kW << 1$, representing a simple model for a *line array*. In these situations Eq. (3) is effectively a 1-D integral along the y-axis using dy_s, and dx_s can be considered a constant representing W.

Beam patterns

We use the Rayleigh integral to study the beam pattern for radiation from a disk of diameter D at particular frequency f and wavelength λ. A common result for this is Eq. (10) from monograph *High Frequency Underwater Sound* in your resource section on the website.

The problem studied is radiation from a disk of diameter 2 m, observed at a set of field points

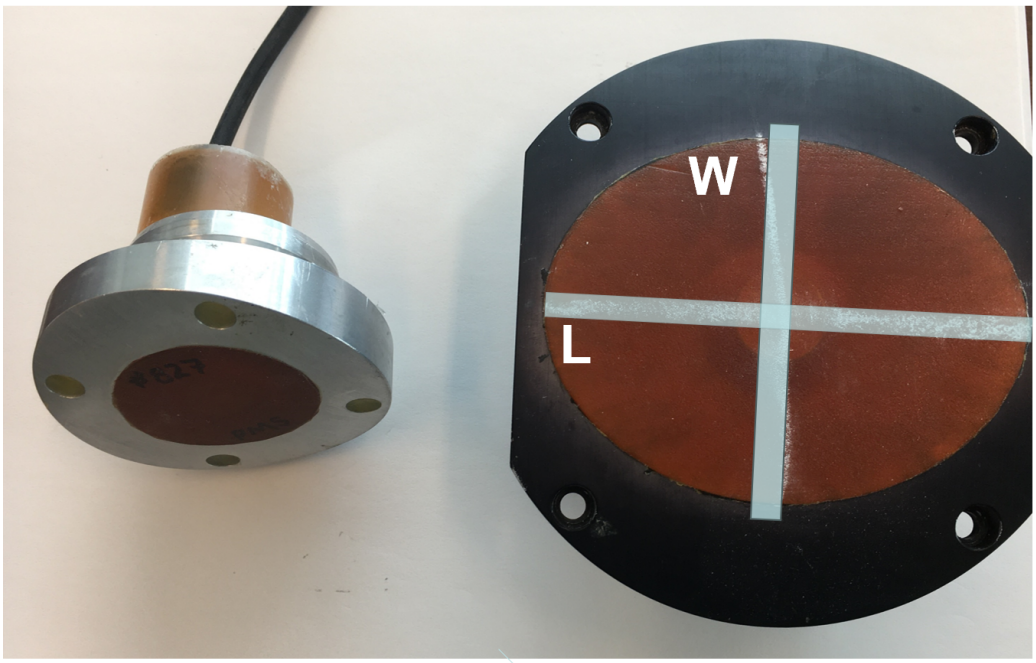

Figure 2: Two planar-like apertures. Right: orange-colored aperture (made of acoustic transparent material) surrounded by a baffle (black); lines identify two characteristic length scales, say L and W of the aperture. Left: smaller aperture surrounded by an metallic frame that serves as the baffled. Both apertures and baffle are slightly curved to fit within the side walls of an AUV.

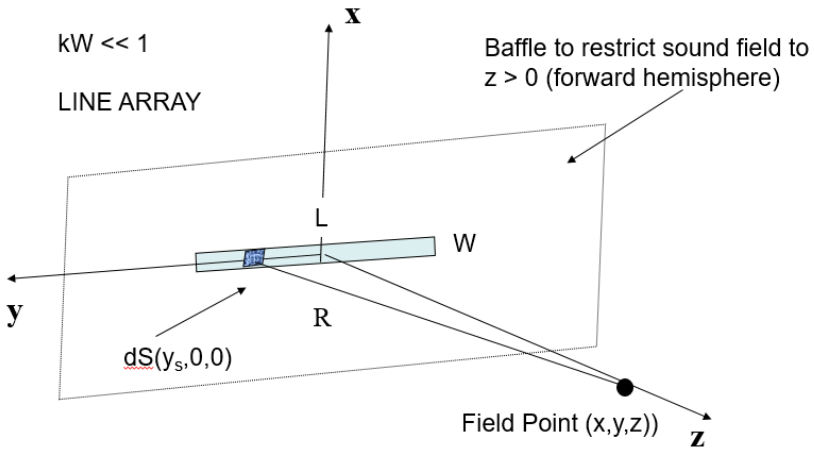

Figure 3: Cartesian coordinate system established at the center of radiating line aperture confined to a baffle to restrict the sound field to $z > 0$. The elemental source dS is distance R from the field point where $R = \sqrt{(y - y_s)^2 + x^2 + z^2}$. Because the aperture width is narrow in the sense of $kW << 1$ the aperture is considered a line array.

all at range 10 m from center of disk but at different angles. A top view [Fig. 4 (a)] shows field points in blue, all having $|\vec{r} - \vec{r}_s|$ equal to 10 m (coordinate axis centered on disk) but differing θ with respect to a line perpendicular to the disk center. Another view [Fig. 4 (b)] the disk looks

solid red, but it is composed of 1200 points, each with elemental area dS, the sum of all elemental areas approximating the total area. Note: strictly speaking, a rigid baffle surrounds the radiating disk. However the baffle is just a convenient conceptual bridge to help justify use of the Rayleigh integral. For many applications as in this case, this feature of the problem can be effectively ignored. The key property is the basic flatness of the aperture.

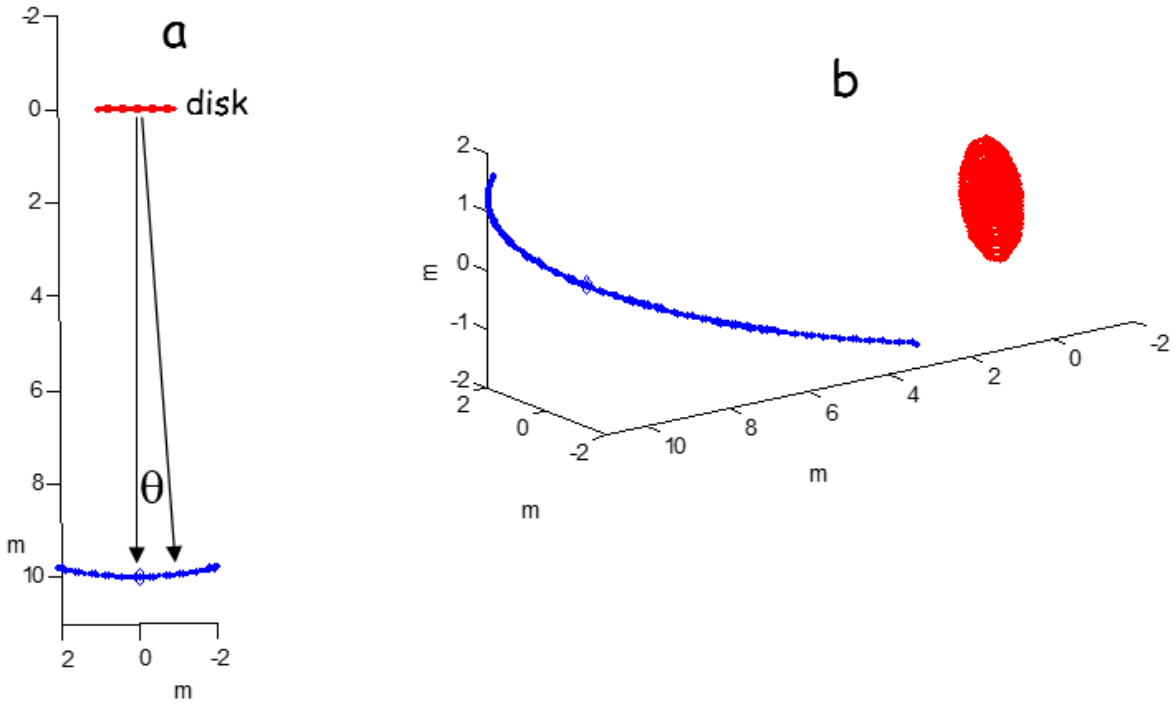

Figure 4: Problem studied: radiation from a disk of diameter 2 m, (a) observed at a set of field points (blue dots) all at range 10 m from center of disk but at different angles θ (b) alternate view showing the red disk and several field points at the same range but varying angle θ. Note that the set of field points align with a line that would divide the disk evenly.

To complete the numerical integral each dS is multiplied by $\frac{-i\omega\rho_0 u_n}{2\pi}\frac{e^{ikR}}{R}$, where R connects a particular dS to the field point, and where u_n is normal velocity on the disk. For many problems u_n is unknown, but can be assumed constant over the face of the radiating aperture. Since the problem involves studying the pressure variation with angle and not the value of pressure *per se* it is not essential to know u_n, which can be set to unity or some notional value to represent u_n. However, the subject of study, pressure variation versus angle and range, is completely embodied by the integral in Eq. (3) while assuming some arbitrary constant value for u_n.

Next define the pressure for $\theta = 0°$ as the *on-axis* pressure as it (generally) will be maximal on the center axis where $\theta = 0°$. Also for this simple disk problem the circular symmetry means angular dependence (called the beam pattern) can be characterized by one angle, θ; more complicated problems require two angles. Evaluate the computed pressure (or quantity proportional to it) from

the Rayleigh integral and express results in decibels as follows

$$20\log_{10}(|p(\theta)|/|p(\theta=0^\circ)|) \tag{4}$$

where pressure is computed at fixed range but variable θ. Plotting Eq. (4) as a function of θ gives a *beam pattern*. One needs to know the beam pattern for design purposes that depend on application, e.g., a high-resolution narrow beam for detail versus broad beam.

Hydrodynamic near field versus Geometric near and far fields

In Lecture 7 the concept of a *near field* $kr << 1$ and *far field* $kr >> 1$ were discussed. Based on an idealized point source of the form $p(r,t) = \frac{A}{r}e^{ikr-i\omega t}$, an effective boundary between these two regions occurs at $kr = 1$, representing a very useful guide. On the $kr < 1$ side kinetic energy (KE) began to exceed potential energy (PE), with difference growing as kr decreased further. Another hallmark of the $kr < 1$ region was that specific acoustic impedance began to go as $-i\omega\rho_0 r$ where r is distance from source, such that the basic property of sound in the form of a sound speed c, was lost. Finally, the acoustic field components, pressure and velocity begin to become 90° out of phase in this region.

At this stage of game it's best to use a more precise language and call the region $kr << 1$ as the *hydrodynamic near field* (Fahy,2001) because here the fluid velocity properties are more similar to hydrodynamic flows, where compression-induced potential energy (characterized by sound speed c) is small relative to kinetic energy. The handy guide for when this happens, $kr < 1$, is still valid.

The hydrodynamic near field has range r from the source as the only length scale, which is parameterized by kr. In the current discussion involving the Rayleigh integral and beam patterns, length scales of the radiating aperture such as length L and width W, or diameter D, influence properties of the acoustic field as function of the range scale r. There is need for new definitions, defined subsequently, which will be known formally as the *geometric near field* and *geometric far field*.

With the above introduction in mind, we continue with discussion of the problem of radiation from a disk of diameter 2 m (Fig. 4). Results (Fig. 5) show calculation at 3 ranges defined by the field point $|\vec{r} - \vec{r}_s|$ equal to 4, 10 and 20 m but with varying θ. Notice that the 10 and 20 m results are quite similar (if not effectively the same) whereas results at 4 m look different. This is because 10 m and beyond represents the geometric far field, also known as the *Fraunhofer zone*. In this example, the geometric far field was determined by acoustic frequency (3000 Hz), medium speed (water 1500 m/s) and radiating aperture size (disk diameter 2 m). Observe also for the case of 10 and 20 m, that the first maximum beyond the main lobe is about 17 dB less than the main lobe of the beam, which is a far field characteristic for all beam patterns for circular disk sound sources, or piston-like sources operating underwater.

At range 4 m the situation is quite different, because range 4 m represents is still within the

geometric near field which is also known as the *Fresnel zone*. At a range or 4 m $kr \sim 50$ for frequency 3000 Hz and sound speed 1500 m, and so this range is considerably beyond the range $kr = 1$.

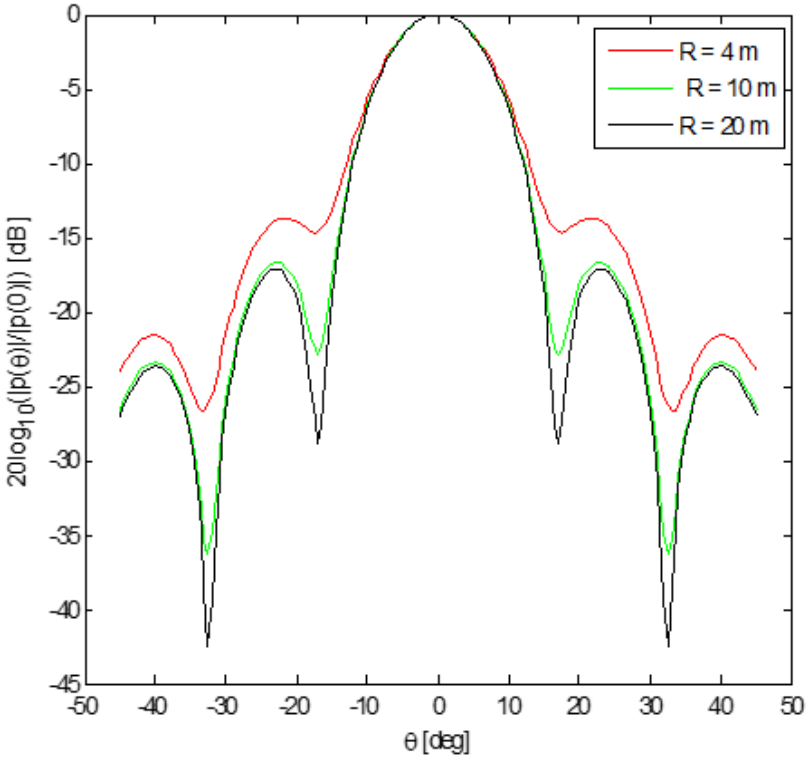

Figure 5: Results from Eq.(3) calculated at 3 ranges defined by the field point $|\vec{r} - \vec{r}_s|$ equal to 4, 10 and 20 m but with varying θ.

Another way of looking at beam patterns is a polar plot (Fig. 6) which is same as Fig. 1 of *High Frequency Underwater Sound* representing a 43 mm diameter disk (called a piston source) with frequency 108 kHz, operating in water. Although the length and frequency scales are very different from the problem just described, observe the first side lobe is also about 17 dB less than the main lobe. Important reminder: here we are using the decibel as comparative metric. Thus we would not write " dB ref. 20μPa (for air), or ref. 1μPa (for water)".

A simple formula $\pi D^2/4\lambda$ defines the critical range where geometric far field (Fraunhofer zone) behavior is expected. For any radiator of characteristic length scale L this formula is L^2/λ. For the case studied this range is ~ 6 m, which explains why the 4 m in Fig. 5 result was in the geometric near field and looked different.

Another handy formula is the beam width of the main lobe for disk transducer. This is the angular width represented by the red, dashed line in Fig. 6, as determined by the angle where the beam pattern has fallen by 3 dB from the maximum (sometimes called the "3 dB" width). This width (in degrees) is $60\lambda/D$ For the example of the 2 m diameter disk the formula gives 15°.

We summarize these handy formulas on party napkins (impress your friends at a party). Use L

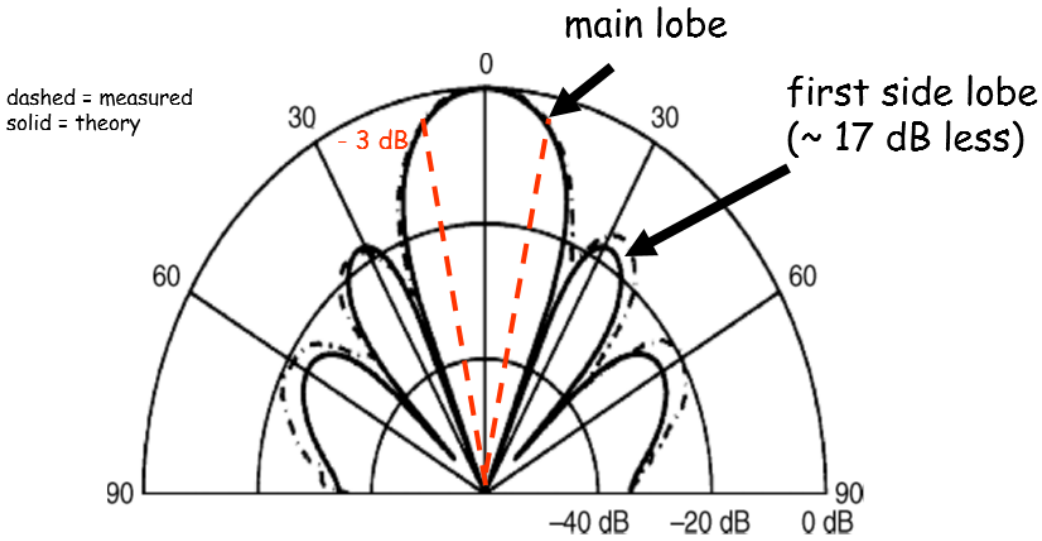

Figure 6: Polar plot of a beam pattern. See also Fig. 1 of High Frequency Underwater Sound.

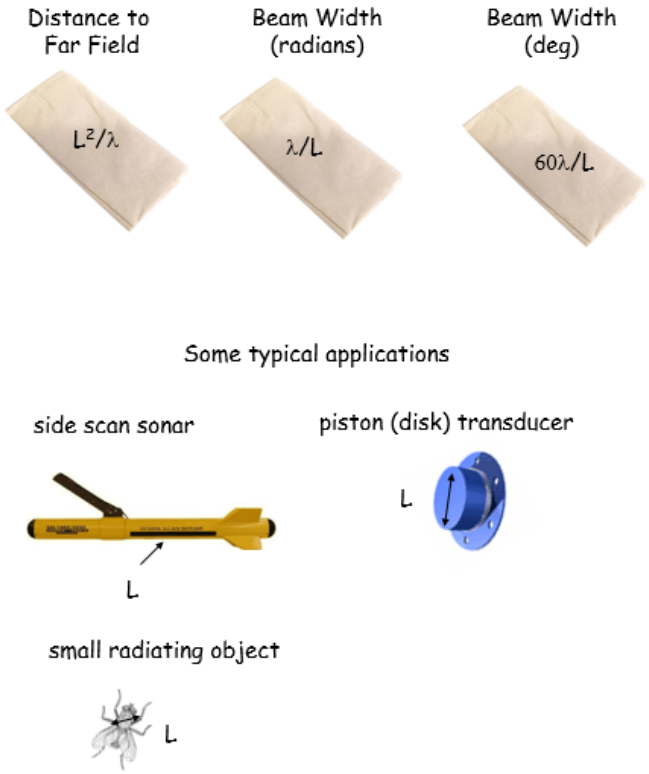

Figure 7: Some basic rules for the distance to the far field and associated beam width of a radiating aperture of length scale L and wavelength λ.

for characteristic scale; for a disk, substitute diameter D for L and the result is nearly exact. Also, further simplify the geometric far field result by noting $\pi/4$ is sufficiently close to 1.

These are valuable for their quick-estimating power–but they can also serve as a check on on a numerical study – if the result of that study differs markedly with these rules you have reason to

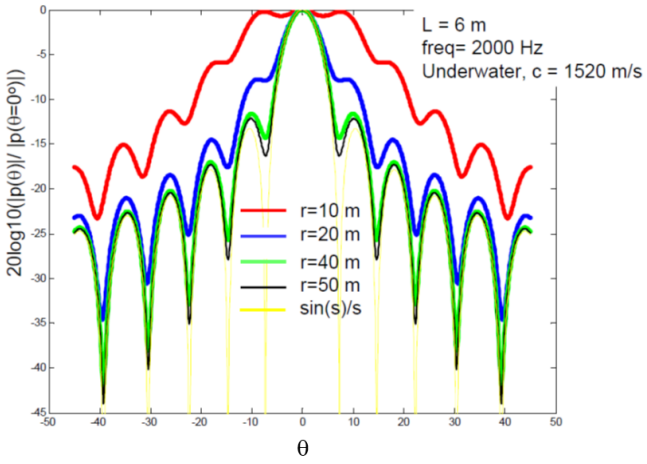

Figure 8: Beam pattern at various ranges from a line array of length 6 m operating in water at frequency 2000 Hz.

question the numerical results. An example involving a line array of length L (Fig. 8) shows the beam pattern evolving with range. For this case L^2/λ is about 47 m, and observe that between 40 and 50 m the beam pattern stabilizes to its geometric far field result. The far field result is $\sin(s)/s$ where $s = \frac{kL}{2}\sin(\theta)$.

Finally, exercise some caution when using this terminology. You might come across to others as being overly particular in using terms like geometric near and far field, when perhaps more experienced professionals might abbreviate these terms as just near and far field while discussing beam patterns and other properties of sound radiation. One solution is to reserve the term *hydrodynamic near field* for the special case of $kr < 1$ and there are otherwise no other length scales such as L, W or D involved, and use *near* and *far field* when such scales are involved.

References

M. C. Junger and D. Feit,*Sound, Structures, and Their Interaction* (Acoustical Society of America, and American Institute of Physics, 1993)
Pierce, A. B, *Acoustics, An Introduction to its Physical Principals and Applications*, (Acoustical Society of America, and American Institute of Physics, 1989). See in particular pp. 213-214.
F. Fahy, *Foundations of Engineering Acoustics* (Elsevier Academic Press, San Diego, CA, 2001)

ME525 Applied Acoustics Lecture 14, Winter 2022
About the Fraunhofer zone and the Rayleigh integral additional numerical details and study of near field far field ranges

Peter H. Dahl, University of Washington

The Fraunhofer zone

Consider an aperture of length L and width W with $kW << 1$, so we need only study the effects of L. At some close range and you measure the radiated pressure (amplitude) as function of angle θ; call this result the function $H1(\theta)$ (Fig. 1). Move on out to another range, and a very different function, $H2(\theta)$ is determined. Now move considerably farther out in range, and a third function $B(\theta)$ is measured; move out some more and the angular dependence has not changed—now you've entered the Fraunhofer zone.

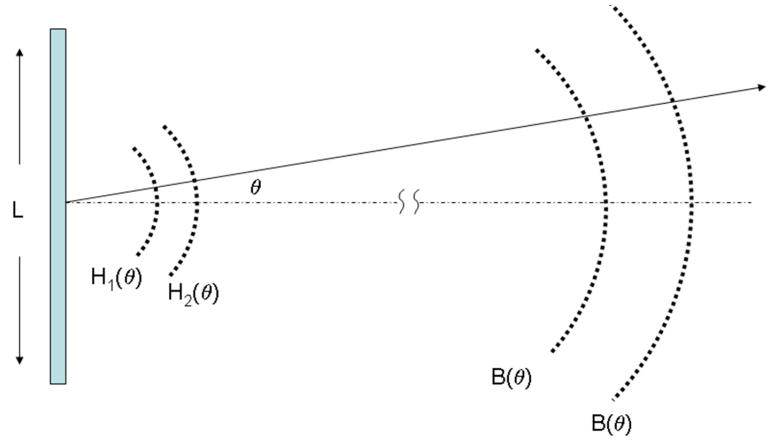

Figure 1: Measures of pressure from the array of length L at four ranges with angular dependence of pressure variation for fixed range

In the Fraunhofer zone:

- angular dependence, $B(\theta)$, does not vary with range,
- pressure is varying as $1/r$, where r is range from the center of the aperture. The function $B(\theta)$ is also called the beam pattern. (More typically $B(\theta)$ is expressed as either its absolute value, or as an intensity beam pattern, $|B(\theta)|^2$).
- $B(\theta)$ has a Fourier transform relation to this aperture geometry, i.e., the longer the L the more narrow the $B(\theta)$.

To understand this, look at a contribution from an elemental source, dp, at the field point (Fig.

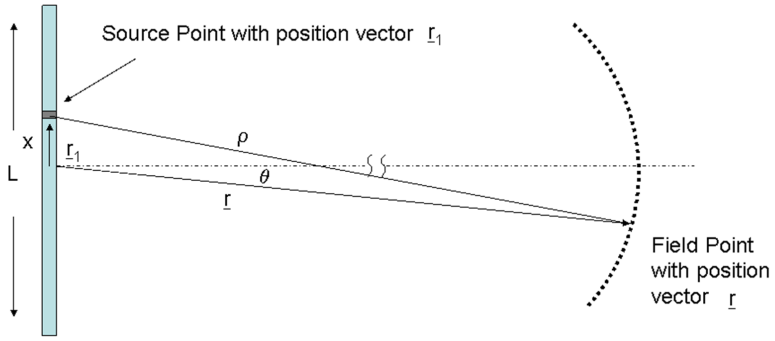

Figure 2: Result of an elemental source measured by a field point in the Fraunhofer zone.

2), where

$$dp = \frac{A}{\rho} e^{ik\rho} dx \tag{1}$$

Let the scalar value ρ be the slant range from the elemental source to the field point which equals $|\vec{r_1} - \vec{r}|$, where $\vec{r_1}$ is the position vector of source point and $\vec{r}$ is that for the field point. At a sufficient distance from the aperture approximate ρ ith the binomial approximation:

$$\rho = |\vec{r}| + x \sin\theta + \frac{x^2}{2|\vec{r}|} \cos^2\theta + ... \tag{2}$$

Taking the first term beyond $|\vec{r}|$ is called the Fraunhofer approximation, and including the next term is called the Fresnel approximation. Continuing with the Fraunhofer approximation,integrate the elemental sources along the line array. For this we write $|\vec{r}|$ as r, with result:

$$p(r,\theta) = \frac{A}{r} e^{ikr} \int_{-L/2}^{L/2} e^{ikx\sin\theta} dx = \frac{A}{r} e^{ikr} \frac{\sin s}{s} \tag{3}$$

where $s = k\frac{L}{2}\sin\theta$ and thus $B(\theta) = \frac{\sin s}{s}$. (The constant A is used to insure Eq.(3) has dimension of pressure, but otherwise it is of no consequence.) Notice that denominator of Eq.(1), which would have been $\rho \approx |\vec{r}| + x\sin\theta$ in the Fraunhofer sense, is further approximated by $\rho \approx r$, allowing $\frac{A}{\rho} e^{ik\rho}$ to be outside the integral in Eq.(3).

Recognize now that integration over the length of the aperture, yielding $B(\theta)$ as a *Fourier transform* of the aperture. As in all Fourier transform relations there is an inverse relation between the Fourier transform variables (e.g., like time and frequency). Here, the longer the aperture length L, the narrower the function $B(\theta)$ becomes.

Typically, angular width is determined as follows: The pressure or intensity are maximal at $\theta = 0$, for which puts $B = 1$, and $20log_{10}|B| = 0$ dB. Find angle θ_{3db} such that $20log_{10}|B(\theta_{3db})|$ = -3 dB; call this the "3 dB half angle" and doubling it gives the nominal angular width of the array. Find

that $\theta = 0$ (in radians) goes at $1/(kL)$, which is consistent with our notion of the Fourier transform inverse relation. In fact, $\theta_{3db} \approx \pi/(kL)$ is a reasonable approximation.

When does the Fraunhofer approximation apply? Consider tEq.(2) and write instead $k\rho = k|\vec{r}| + kx\sin\theta$. This requires $k\frac{x^2}{2|\vec{r}|} << 1$ since the $\cos$ factor is always order unity. As the maximum extent of x equals $L/2$, we should incorporate L into the bound. This requires r being much greater than $k\frac{L^2}{8}$. In practice this bound will be nominally satisfied with $r > L^2/\lambda$.

Numerical implementation of the Rayleigh Integral

A typical example for the Rayleigh integral in Eq. (1) is shown in Fig. 3

$$p(\vec{r}) = \frac{-i\omega\rho_0}{2\pi}\int_S u_n(x_s, y_s)\frac{e^{ikR}}{R}dx_s dy_s \tag{4}$$

where $R = |\vec{r} - \vec{r}_s|$. With few exceptions this is implemented numerically, the most common method through a summation from each contribution originating from area dS.[1] It is essential to properly size the elemental area dS, otherwise there will numerical errors in approximating the Rayleigh integral. From our previous notion of a monopole source of radiation area A, we anticipate a requirement that $\sqrt{dS} << \lambda$.

Now let's assume kW is not $<< 1$, and there is a rectangular array of area LW. The same ideas apply, the new rule for transition to Fraunhofer zone is $r > \frac{LW}{\lambda}$, and there is of course another beam pattern function that relates to kW. The combined beam pattern function is the product of the two sinc functions.

It's useful to compare numerical results with an exact solution for the beam pattern of a line array in the geometric far field (this being $\sin(s)/s$ where $s = \frac{kL}{2}\sin(\theta)$). Figure 4 shows $B(\theta)$ for a line array of $L = 2$ m, operating at 5000 Hz in water. This is a 1D integral so here the dS is effectively determined by dy_s, and the "length scale" of an elemental source is dy_s.

Three attempts are made as parameterized by kdy_s, and it should be clear that we need to have $kdy_s < 1$ to get acceptable results. For the case of $kdy_s = 0.21$ there is effectively no difference between the numerical and exact result. The experiment is repeated at higher frequency 8000 Hz (Fig. 5) giving a different set of three kdy_s values, showing that $kdy_s = 0.34$ is also close. Also observe the reduced beam width for 8000 Hz, as defined by angular width of the main lobe, or alternatively, width to the first null.

In summary the results suggest this rule: $kdy_s < 0.2$ for 1D line array study, and $k\sqrt{S} \leq 0.2$ for 2D study as in Fig. 3 which is of course consistent with the original conjecture of $\sqrt{dS} << \lambda$.

Range dependence and the near and far fields

[1] The term for this is a Riemann summation; see Foote,(2014).

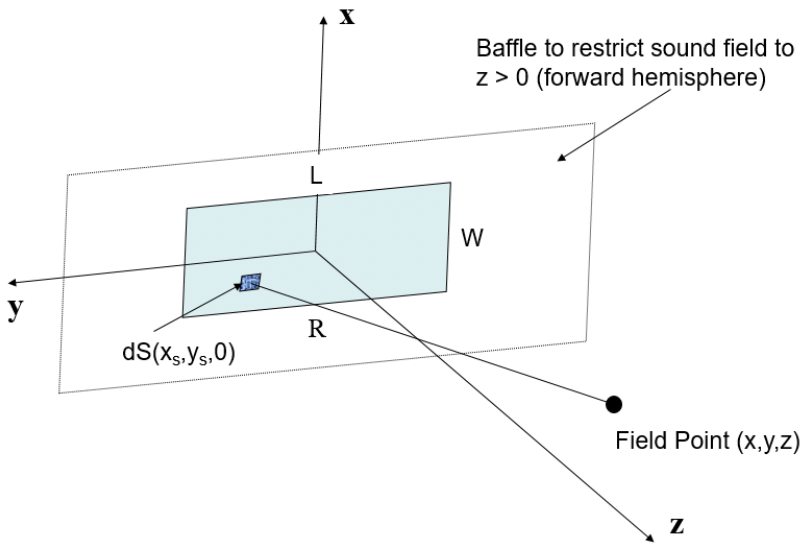

Figure 3: Cartesian coordinate system established at the center of radiating rectangular aperture confined to a baffle to restrict the sound field to $z > 0$. The elemental source dS is distance R from the field point where $R = \sqrt{(x - x_s)^2 + (y - y_s)^2 + z^2}$

The field on the acoustic axis of a rectangular array of $L = 1.5$ m, $W = 2$ m, is plotted as a function of range (Fig. 6), showing the complicated pattern that develops immediately in front of the array: this is the *near field*. With increasing range away from the aperature the field settles down into more smooth decay: this is the *far field*. Here pressure goes as $\sim 1/R$–or the inverse range spreading we would have expected all along from a compact point source.

The near field-far field transition is well predicted by the basic guide LW/λ. For nearly all applications, this transition must be well understood. For example, in a system calibration of this array it is desirable to place a test acoustic source (or acoustic receiver) in the far field to either receive from or transmit signals to this array. Thus, it is essential to know, with confidence, that this position is indeed in the far field because here the pressure field has simplified behavior, going as $\sim 1/R$ (dotted line in Fig. 6), and it is straightforward to correct measurement made at different ranges.

Next let us examine the 2D angular properties in the acoustic field, here using a rectangular array of $L = 1.2$ m, $W = 0.6$ m, again operating at 5000 Hz in water (Fig. 7). These calculations are made well into the far field (i.e., range $>> LW/\lambda$), and you should by now have an intuitive feel for the results.

For one case in Fig. 7, θ sweeps across the L dimension such that $\theta = 0^\circ$ aligns with z axis and $\theta = 90^\circ$ aligns with y axis; for the other case θ sweeps across the W dimension such that $\theta = 90^\circ$ aligns with x axis (see also Fig. 3). Since $L > W$ we expect the beam width across L to be more narrow than that across the W dimension, consistent with the Fourier relation between aperture scale and angular width. Since the calculations are made well in the far field the $\sin(s)/s$ associated

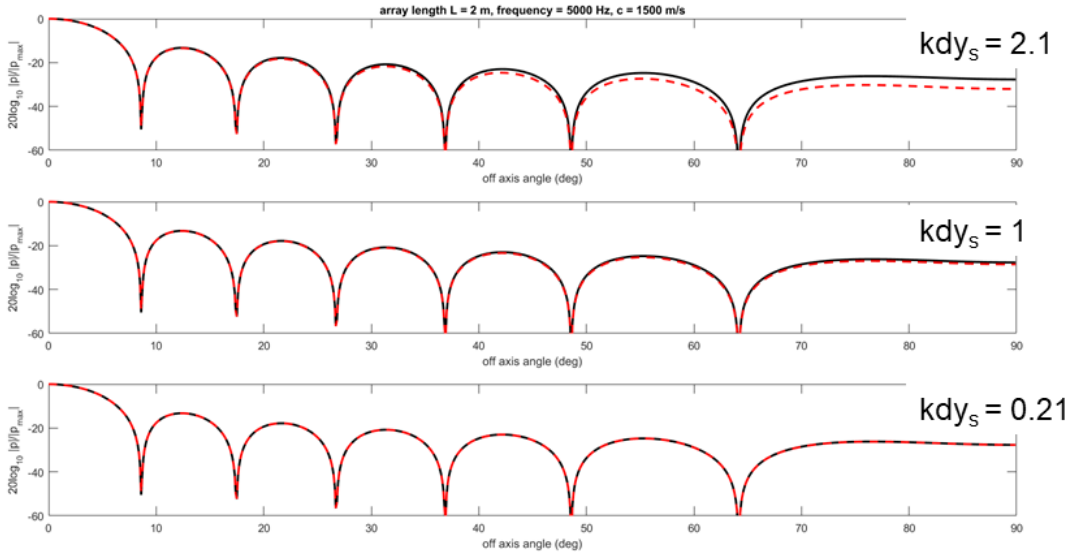

Figure 4: beam pattern $B(\theta)$ as expressed by $20\log_{10}|p(\theta)|/|p_{max}|$ computed in the far field of a line array of length 2 m, frequency 5000 Hz in water. Dashed, red line is the result computed using the identified kdy_s giving size of dy_s and solid, black line is theoretical result.

with each dimension predicts the beam pattern quite well, where s is either $\frac{kL}{2}\sin(\theta))$ or $\frac{kW}{2}\sin(\theta)$. Figure 8 shows the beam pattern as if looking straight into the beam at some position in far field. Because the long side L is oriented horizontally, the beam appears more narrow in this direction.

Array shading and a practical application of the Rayleigh Integral in Medical Ultrasound

A simple demonstration of aperture (or array) shading is illustrated in Fig. 9. An aperture about 15 by 21 cm is shown on the left side. The unshaded narrow beam based on the full 15 by 21 cm dimension is shown by the red beam pattern on the right side. We can shade this aperture in a simple way by by setting all sources, as in $u_n(x_s, y_s)$ of Eq.(4), to 0, for source locations on the corners of the aperture. The shaded aperture is shown by the black on left side and corresponding beam pattern on right side. The total length of the shaded aperture is still the same but you can see that the shaded beam pattern has broadened somewhat and side lobes have been reduced.

There are many applications where this result is desirable and the Rayleigh integral can be

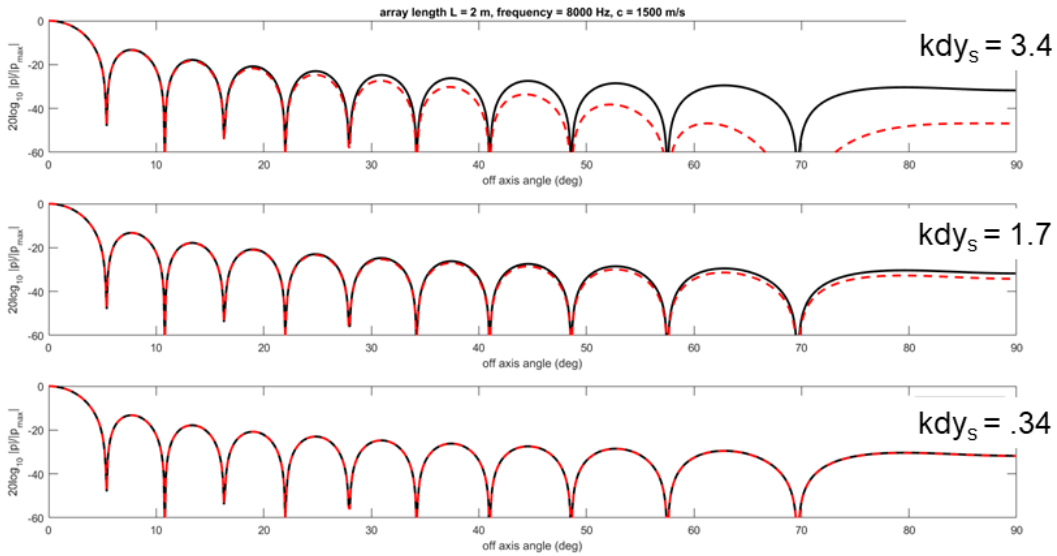

Figure 5: Beam pattern $B(\theta)$ as expressed by $20\log_{10}|p(\theta)|/|p_{max}|$ computed in the far field of a line array of length 2 m, frequency 8000 Hz in water. Dashed, red line is the result computed using the identified kdy_s giving size of dy_s and solid, black line is theoretical result.

used as an exploratory tool find an optimal solution. A more sophisticated example of this is provided by Dr. Wayne Kreider of the Applied Physics Laboratory's Center for Industrial and Medical Ultrasound. In this case the aperture is composed of 256 elements arranged in a spiral (Fig. 10) which at the transmit frequency of 1.5 MHz, produces a focus point at about 120 mm away on the acoustic axis (Fig. 11). Keep in mind that given the combination of element diameter d of 7 mm, and the high frequency 1.5 MHz, puts $kd >> 1$ and thus a Riemann summation with appropriately small dS must be applied to each of the 256 elements. More on this study can be found in Kreider, *et al.* (2018).

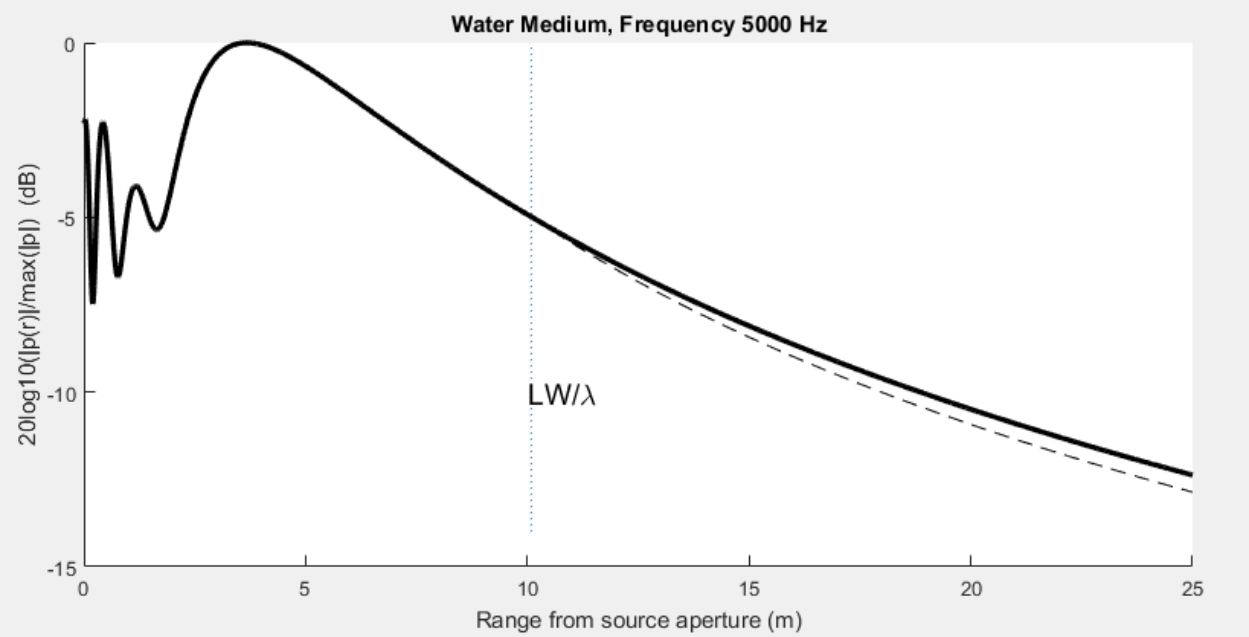

Figure 6: Relative magnitude of pressure field (expressed dB) on the acoustic axis of a rectangular array of array of $L = 1.5$ m, $W = 2$ m as function of range, for frequency 5000 Hz operating in water. The near-far field transition point is shown at range = LW/λ, after the pressure magnitude goes as $\sim 1/R$

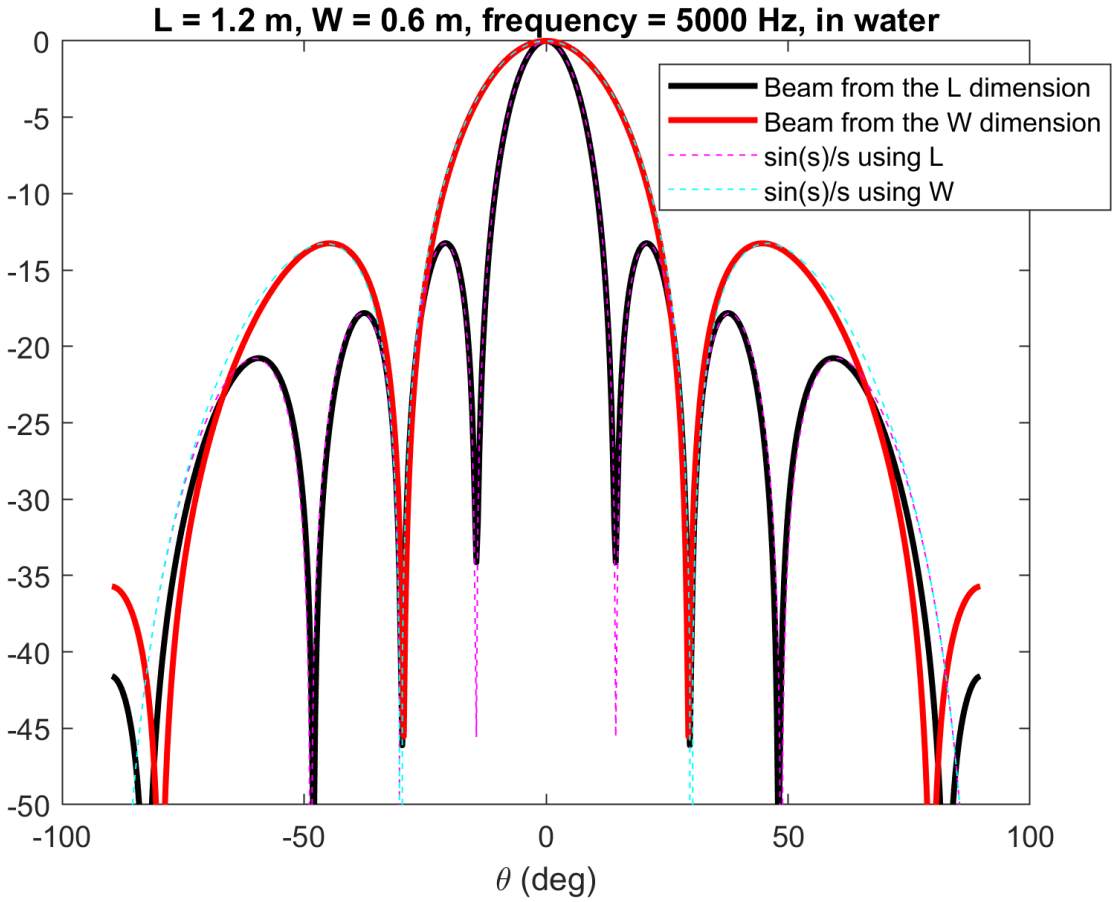

Figure 7: Relative magnitude of pressure field (expressed dB) on the acoustic axis of a rectangular array of array of $L = 1.2$ m, $W = 0.6$ m as function of angle θ, for frequency 5000 Hz operating in water. For one case θ sweeps across the L dimension such that $\theta = 0^\circ$ aligns with z axis and $\theta = 90^\circ$ aligns with y axis; for the other case θ sweeps across the W dimension such that $\theta = 90^\circ$ aligns with x axis. See Fig. 1 for geometry.

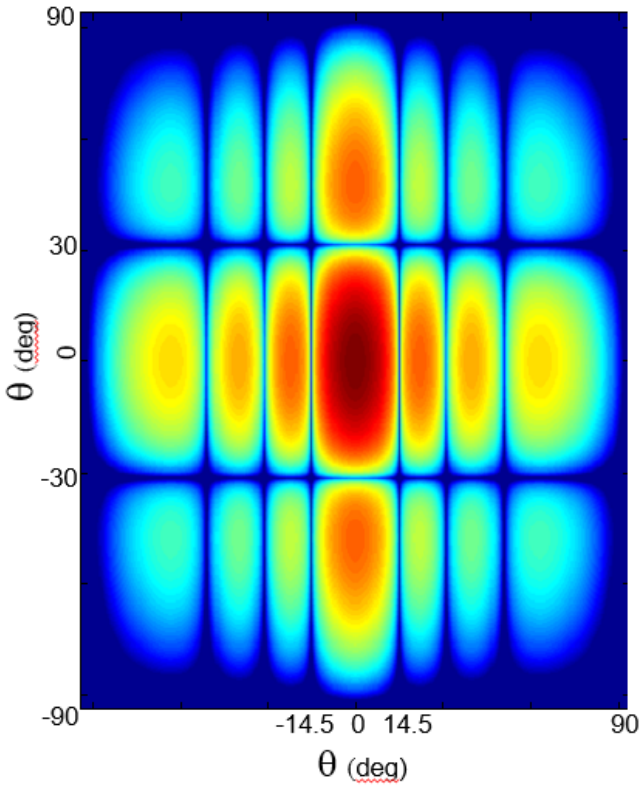

Figure 8: Beam pattern from example in Fig. 7 as if looking straight into the beam at some position in far field. Red-to-blue denotes high-to-low levels of the beam pattern. The beam originates from an aperture shown in Fig. 3. Because the long side L is oriented horizontally, the beam appears more narrow in this direction.

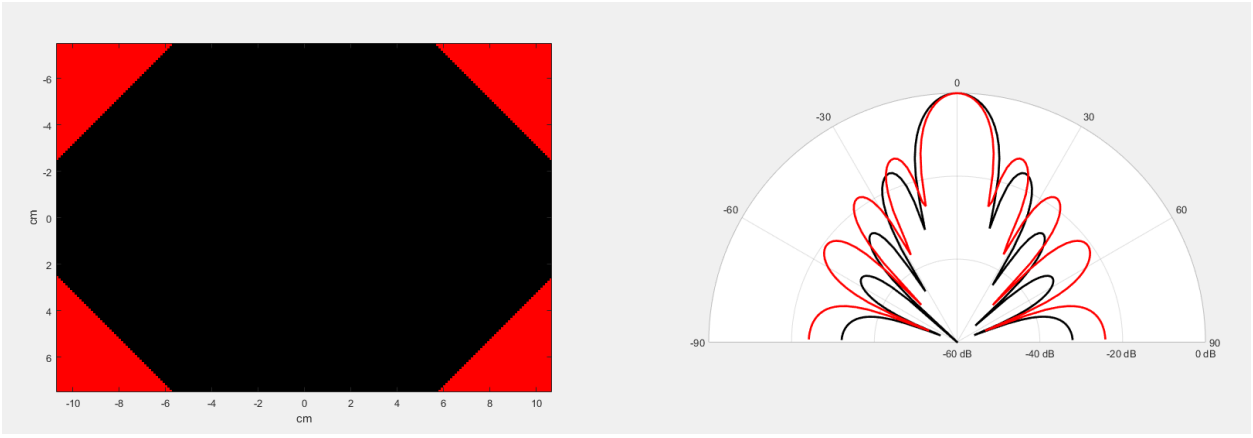

Figure 9: left side: shaded aperture (black) and unshaded aperture (red + black). Right side: Beam pattern computed in the far field for frequency 30 kHz, representing pattern for the long axis of the aperture, for shaded aperture (black) and unshaded aperture (red).

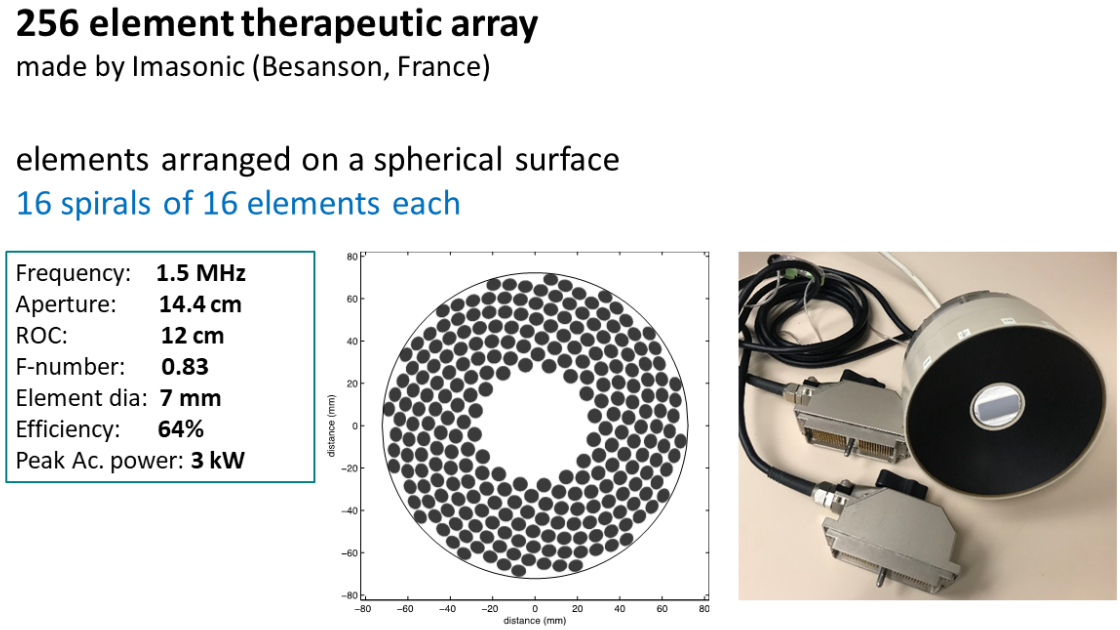

Figure 10: 256 element spiral array used for focused ultrasound applications in diagnostic and therapeutic applications in medical ultrasound.

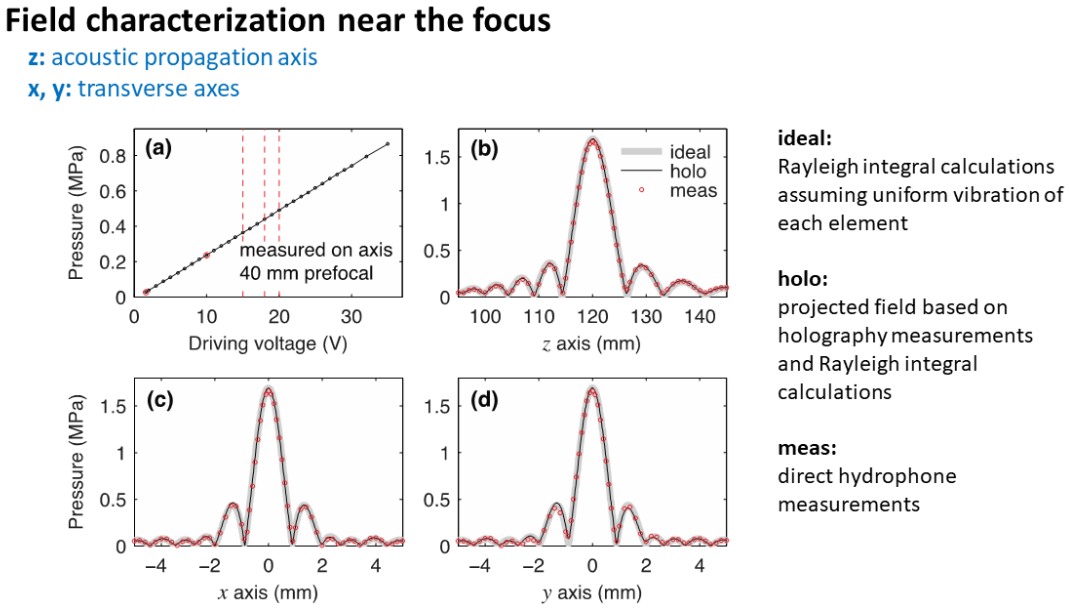

Figure 11: Field characterization near the focus points based on the Rayleigh integral (thick, gray lines) compared with measurement.

References

K.G. Foote , "Discriminating between the nearfield and the farfield of acoustic transducers," *J. Acoust. Soc. Am.* 136, October 2014.

W. Kreider *et al.*, "Characterization of Multi-Element Clinical HIFU System Using Acoustic Holography and Non-linear Modeling," *IEEE Transactions on Ultrasonics, Ferroelectrics, and Frequency Control* 60, August 2018.